International Journal of Nanomedicine

Dovepress
open access to scientific and medical research

Open Access Full Text Article

ORIGINAL RESEARCH

UV photofunctionalization promotes nano-biomimetic apatite deposition on titanium

This article was published in the following Dove Press journal:
International Journal of Nanomedicine
12 January 2016
Number of times this article has been viewed

Makiko Saita[1]
Takayuki Ikeda[1,2]
Masahiro Yamada[1,3]
Katsuhiko Kimoto[4]
Masaichi Chang-Il Lee[5]
Takahiro Ogawa[1]

[1]Division of Advanced Prosthodontics, Weintraub Center for Reconstructive Biotechnology, UCLA School of Dentistry, Los Angeles, CA, USA; [2]Department of Complete Denture Prosthodontics, Nihon University School of Dentistry, Yokosuka, Japan; [3]Division of Molecular and Regenerative Prosthodontics, Tohoku University Graduate School of Dentistry, Sendai, Miyagi, Japan; [4]Department of Prosthodontics and Oral Rehabilitation, [5]Yokosuka-Shonan Disaster Health Emergency Research Center and ESR Laboratories, Kanagawa Dental University Graduate School of Dentistry, Yokosuka, Japan

Background: Although biomimetic apatite coating is a promising way to provide titanium with osteoconductivity, the efficiency and quality of deposition is often poor. Most titanium implants have microscale surface morphology, and an addition of nanoscale features while preserving the micromorphology may provide further biological benefit. Here, we examined the effect of ultraviolet (UV) light treatment of titanium, or photofunctionalization, on the efficacy of biomimetic apatite deposition on titanium and its biological capability.

Methods and results: Micro-roughed titanium disks were prepared by acid-etching with sulfuric acid. Micro-roughened disks with or without photofunctionalization (20-minute exposure to UV light) were immersed in simulated body fluid (SBF) for 1 or 5 days. Photofunctionalized titanium disks were superhydrophilic and did not form surface air bubbles when immersed in SBF, whereas non-photofunctionalized disks were hydrophobic and largely covered with air bubbles during immersion. An apatite-related signal was observed by X-ray diffraction on photofunctionalized titanium after 1 day of SBF immersion, which was equivalent to the one observed after 5 days of immersion of control titanium. Scanning electron microscopy revealed nodular apatite deposition in the valleys and at the inclines of micro-roughened structures without affecting the existing micro-configuration. Micro-roughened titanium and apatite-deposited titanium surfaces had similar roughness values. The attachment, spreading, settling, proliferation, and alkaline phosphate activity of bone marrow-derived osteoblasts were promoted on apatite-coated titanium with photofunctionalization.

Conclusion: UV-photofunctionalization of titanium enabled faster deposition of nanoscale biomimetic apatite, resulting in the improved biological capability compared to the similarly prepared apatite-deposited titanium without photofunctionalization. Photofunctionalization-assisted biomimetic apatite deposition may be a novel method to effectively enhance micro-roughened titanium surfaces without altering their microscale morphology.

Keywords: nanotechnology, dental and orthopedic implants, superhydrophilic, hydrocarbon, osseointegration

Introduction

Coating or depositing hydroxyapatite on titanium has been used to enhance the bioactivity and osteoconductivity of titanium surfaces and improve bone-to-titanium integration.[1,2] Various biomaterials have been immersed in simulated body fluid (SBF) to form biomimetic apatite of similar chemical composition and molecular structure to bone on the material surface.[2–4] Significant progress has been made in depositing biomimetic apatite on titanium-based materials;[1,4–7] however, the speed, efficiency, and quality of biomimetic apatite formation tend to be insufficient for commercial implant purposes. To date, titanium materials have been pretreated with water, acidic and alkaline chemicals, thermal and electrochemical oxidation, or their combination to improve apatite deposition.[4,6,8–11] Other technologies, such as single- and multiple-layer splat

Correspondence: Takahiro Ogawa
Weintraub Center for Reconstructive Biotechnology, Division of Advanced Prosthodontics, Biomaterials and Hospital Dentistry, UCLA School of Dentistry, 10833 Le Conte Avenue (B3-081 CHS), Box 951668, Los Angeles, CA 90095-1668, USA
Tel +1 310 825 0727
Fax +1 310 8256345
Email togawa@dentistry.ucla.edu

technique, and thermal printing, are also available to improve the mechanical properties of the apatite coating.[12–14]

From the perspective of titanium medical implants, it remains challenging to add beneficial nanoscale structures without altering the existing microscale morphology.[15–24] Many currently used implant surfaces have microscale roughness or topography that are known to enhance the biological and biomechanical capabilities and improve clinical outcomes compared to relatively smoother surfaces, such as a machined surface.[21,25,26] The microscale morphologies used in commercial implants include compartmental structures with peaks and valleys, pores, and other irregular structures produced by acid-etching, chemical and thermal oxidization, sandblasting, or their combination.[21,25–28] Adding nanoscale morphology to microscale morphology may improve osteoconductivity and mechanical interlocking between titanium and bone.[16,29] Unfortunately, the methods currently used to improve biomimetic apatite deposition substantially alter the microscale morphology of titanium surfaces.

Treatment of titanium with ultraviolet (UV) light immediately prior to use, or photofunctionalization, increases the biological capability and osteoconductivity of titanium.[30–36] Photofunctionalization is neither additive nor subtractive, since it does not alter the surface morphology of titanium. Instead, physicochemical properties of titanium are significantly improved by photofunctionalization.[30,31] Carbon-containing impurities, primarily consisting of hydrocarbon, which had been unavoidably accumulated on titanium surfaces, are decomposed and removed by photofunctionalization.[30,33,37] Because of carbon removal, titanium surfaces change from hydrophobic to super-hydrophilic.[30,31,33] The surface charge also changes from electronegative to electropositive.[35,38] Photofunctionalization-induced super-hydrophilic titanium surfaces help avoid trapping air bubbles when exposed to blood and create a hemophilic environment, providing proteins and cells with maximum access to titanium.[30,31] Next, the electropositivity of the surface works as a surface attractant, bringing more proteins and osteogenic cells to the titanium surface because they are negatively charged.[35,38,39] Finally, clean titanium surfaces with less carbon facilitate the attachment and settlement of cells and promote their proliferation, leading to the acceleration and enhancement of bone formation.[30,31,33,40] Photofunctionalization has been proven useful and effective in dental implant therapy.

We hypothesized that titanium surface pretreatment with UV-photofunctionalization would enhance biomimetic apatite deposition. In addition, we aimed to establish nanoscale biomimetic apatite deposition on micro-roughened surfaces without altering the existing microscale configuration. The objective of this study was to characterize biomimetic apatite deposition on micro-roughened titanium with and without photofunctionalization.

Materials and methods

Titanium samples and photofunctionalization

Commercially pure grade 2 titanium disks (20 mm diameter, 1.5 mm thickness) were machine-prepared and acid-etched with 67% H_2SO_4 at 120°C for 75 seconds. The biological capability of titanium is known to undergo age-dependent degradation, or "biological aging".[37,41] Therefore, titanium disks were stored for 4 weeks to standardize the aging effect after acid etching.

Titanium disks were photofunctionalized with UV light for 20 minutes (15 W bactericidal lamp; Toshiba, Tokyo, Japan). This light source has a combined peak intensity of 0.05 mW/cm^2 (λ=360±20 nm) and 2 mW/cm^2 (λ=250±20 nm). Surface morphology was examined using scanning electron microscopy ([SEM] XL30; Philips, Eindhoven, the Netherlands) and laser profiling microscopy (VK-8500; Keyence, Osaka, Japan) for Sa (average roughness), Sq (root-mean-square roughness), Sz (peak-to-valley roughness), Ssk (skewness roughness), and Sku (kurtosis roughness). Surface chemistry was examined by X-ray photoelectron spectroscopy (ESCA3200; Shimadzu, Tokyo, Japan). The wettability of titanium surfaces was evaluated by measuring the contact angle of 10 µL of H_2O.

Biomimetic apatite deposition and characterization

Acid-etched titanium disks with or without photofunctionalization were soaked in SBF (pH 7.40) at 37°C for 1 day or 5 days. Following an established method,[1] SBF was prepared to mimic the ion concentrations found in human plasma. After being removed from SBF, the disks were gently washed three times in distilled water by stirring for 30 seconds and then air-dried on a clean bench. SEM was then used to assess surface morphology as described earlier. Calcium phosphate deposition was assessed by X-ray diffraction (XRD) (MiniFlex II; Rigaku, Tokyo, Japan) and calcium deposition assay. For the calcium deposition assay, the titanium disks were washed with phosphate buffered saline and incubated overnight in 1 mL 0.5 M HCl solution with gentle shaking. The solution was mixed with *o*-cresolphthalein complexone in alkaline medium (Calcium Binding and Buffer Reagent; Sigma-Aldrich Co., St Louis, MO, USA) to produce a red calcium–cresolphthalein complexone complex. Color intensity was measured using a microplate reader (Synergy

HT; BioTek Instruments, Winooski, VT, USA) at 575 nm absorbance.

Osteoblast culture

Osteoblasts were cultured on titanium disks to examine their biological capability as previously described.[42] Briefly, bone marrow cells isolated from the femurs of 8-week-old male Sprague-Dawley rats were inoculated into alpha-modified Eagle's medium supplemented with 15% fetal bovine serum, 50 μg/mL ascorbic acid, 10 mM Na-β-glycerophosphate, 10^{-8} M dexamethasone, and antibiotic-antimycotic solution. Cells were incubated in a humidified atmosphere of 95% air and 5% CO_2 at 37°C. Cells were detached at 80% confluency using 0.25% trypsin-1 mM ethylenediaminetetraacetic acid-4Na and then seeded onto titanium disks at a density of 3×10^4 cells/cm^2. The culture medium was renewed every 3 days.

The protocol was approved by the Chancellor's Animal Research Committee at the University of California at Los Angeles (UCLA), and all experimentation was performed in accordance with the United States Department of Agriculture (USDA) guidelines on animal research.

Cell attachment and proliferation assays

The initial attachment of cells to biomimetic apatite-coated titanium disks was evaluated by measuring the number of cells attached to the surfaces after a 24-hour incubation. The density of propagated cells was quantified on day 3 of culture. These quantifications were performed using a tetrazolium salt (WST-1)-based colorimetric assay (WST-1; Hoffman-La Roche Ltd., Basel, Switzerland). A culture well was incubated at 37°C for 4 hours with 100 μL WST-1 reagent. The amount of formazan produced was measured at 420 nm using an enzyme-linked immunosorbent assay (ELISA) reader (Synergy HT; BioTek Instruments). The proliferative activity of cells was also measured by incorporating BrdU during DNA synthesis. On day 3 of culturing, 100 μL of 100 mM BrdU solution (Hoffman-La Roche Ltd.) was added to the culture wells followed by incubation for a further 10 hours. After trypsinizing the cells and denaturing DNA, cultures were incubated with an anti-BrdU conjugated with peroxidase for 90 minutes and reacted with tetramethylbenzidine for color development. Absorbance was measured at 370 nm using an ELISA reader.

Cell morphology and morphometry

Confocal laser scanning microscopy was used to examine the spreading behavior of osteoblasts seeded onto titanium surfaces. Twenty-four hours after seeding, cells were fixed in 10% formalin and stained with rhodamine phalloidin (actin filament, red color; Molecular Probes, Eugene, OR, USA). To visualize the intracellular expression and localization of vinculin, a focal adhesion protein, cells were stained with mouse anti-vinculin monoclonal antibodies (Abcam, Cambridge, UK) and visualized with fluorescein isothiocyanate-conjugated anti-mouse secondary antibodies (Abcam). The area, perimeter, and Feret's diameter were quantified using image analysis software (ImageJ, NIH, Bethesda, MD, USA). Actin and vinculin expression intensities were also quantified.

ALP activity

Alkaline phosphatase (ALP) activity of osteoblasts cultured on titanium disks was examined on day 10 using image- and colorimetry-based assays. For the image analysis, cultured cells were washed twice with Hanks' solution and then incubated with 120 mM Tris buffer (pH 8.4) containing 0.9 mM naphthol AS-MX phosphate and 1.8 mM fast red TR for 30 minutes at 37°C. The ALP-positive area on the stained images was calculated as [(stained area/total dish area) ×100)](%) using an image analyzer (ImageJ). For colorimetry, cells were rinsed with double distilled H_2O, followed by the addition of 250 μL of *p*-nitrophenylphosphate (LabAssay ATP, Wako Pure Chemical Industries, Ltd., Osaka, Japan), and then incubated at 37°C for 15 minutes. ALP activity was evaluated as the amount of nitrophenol released by the enzymatic reaction and measured using an ELISA reader at 405 nm.

Statistical analyses

All biological experiments and chemical analyses, including XRD analysis and calcium deposition assay, were performed in triplicate (n=3) except for cell morphometry (n=9). One-way analysis of variance was used to examine the difference in surface roughness parameters between experimental groups: acid-etched titanium, acid-etched and biomimetic apatite-coated titanium, and acid-etched, photofunctionalized, and biomimetic apatite-coated titanium. Student's *t*-test was used to compare apatite deposition and biological parameters between biomimetic apatite-coated titanium disks with and without photofunctionalization. $P<0.05$ was considered statistically significant.

Results

Surface properties of titanium disks with or without photofunctionalization

Titanium disks were morphologically and physicochemically characterized prior to biomimetic apatite coating. Low-magnification SEM showed that the titanium disks were of uniform roughness, typical for acid-etched titanium (Figure 1A, left image). At high magnification,

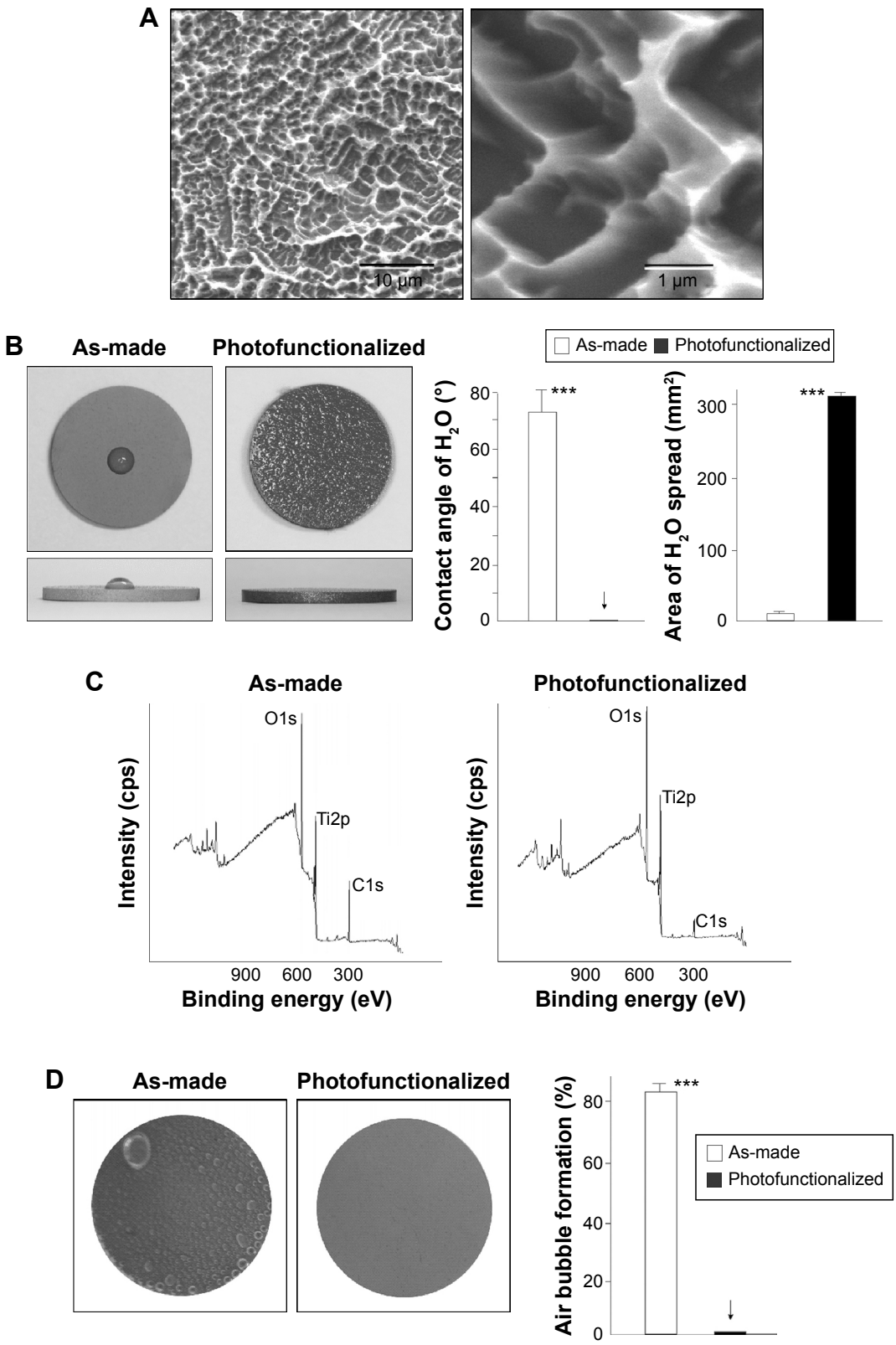

Figure 1 Surface characterization of titanium disks with or without photofunctionalization.

Notes: (**A**) Low- (left) and high- (right) magnification SEM images of acid-etched titanium surfaces used in this study. (**B**) Top- and side-photographic views of 10 µL ddH_2O placed on as-made (acid-etched) and photofunctionalized (acid-etched and photofunctionalized) titanium disks. The calculated contact angle and the area of spread of ddH_2O droplet are also shown. ***$P<0.001$, significant difference between as-made and photofunctionalized titanium. (**C**) XPS spectra of titanium surfaces with or without photofunctionalization. (**D**) Air bubble formation on titanium surfaces after 1-day immersion in SBF. Representative photographic images of titanium disks are shown (left). The coverage of air bubbles is quantified relative to the titanium area in %. ***$P<0.001$, significant difference between as-made and photofunctionalized titanium. The arrows in **B** and **D** denotes the value was 0.0±0.0.

Abbreviations: SEM, scanning electron microscopy; XPS, X-ray photoelectron spectroscopy; SBF, simulated body fluid.

compartmental structures consisting of sharp peaks and valleys were observed; compartment size ranged from 0.5 to 2 μm (Figure 1A, right image). There was a marked difference in wettability before and after photofunctionalization (Figure 1B): a 10 μL ddH_2O droplet placed on as-made titanium disks remained hemispheric, indicating surface hydrophobicity, while water placed onto photofunctionalized disks spread immediately over almost the entire area of the disk, indicating surface superhydrophilicity. The ddH_2O contact angle was greater than 70° on as-made titanium surfaces and 0° on photofunctionalized surfaces.

In X-ray photoelectron spectroscopy chemical analysis, three expected elements were present on titanium surfaces: titanium, oxygen, and carbon (Figure 1C). There was a significant reduction in the atomic percentage of carbon on photofunctionalized titanium disks (8.7%) compared to as-made disks (44.0%). Furthermore, after being soaked in SBF for 1 hour, there were no air bubbles on photofunctionalized disks, whereas most of the as-made disk surfaces (>80%) were covered with air bubbles (Figure 1D).

Formation of biomimetic apatite on titanium

The surfaces of as-made and photofunctionalized titanium surfaces soaked in SBF for 1 day were similar by low-magnification SEM (Figure 2A), with no significant differences in morphology from the original acid-etched surface and the innate microscale peaks and valley topography remaining. However, at high magnification, SBF immersion-related changes were visible on both as-made and photofunctionalized surfaces (Figure 2B). Unique nodular structures were visible at the inclines and tops of peaks. These nodules were smaller than the microscale compartments and colonized within existing structures without altering the microscale configuration. Nano-nodular structure formation appeared to be denser and more extensive on photofunctionalized surfaces than as-made surfaces.

The surface morphology of original acid-etched titanium and SBF-immersed as-made and photofunctionalized surfaces was similar in three-dimensional profiling images (Figure 3A). Quantitative morphometric analysis confirmed

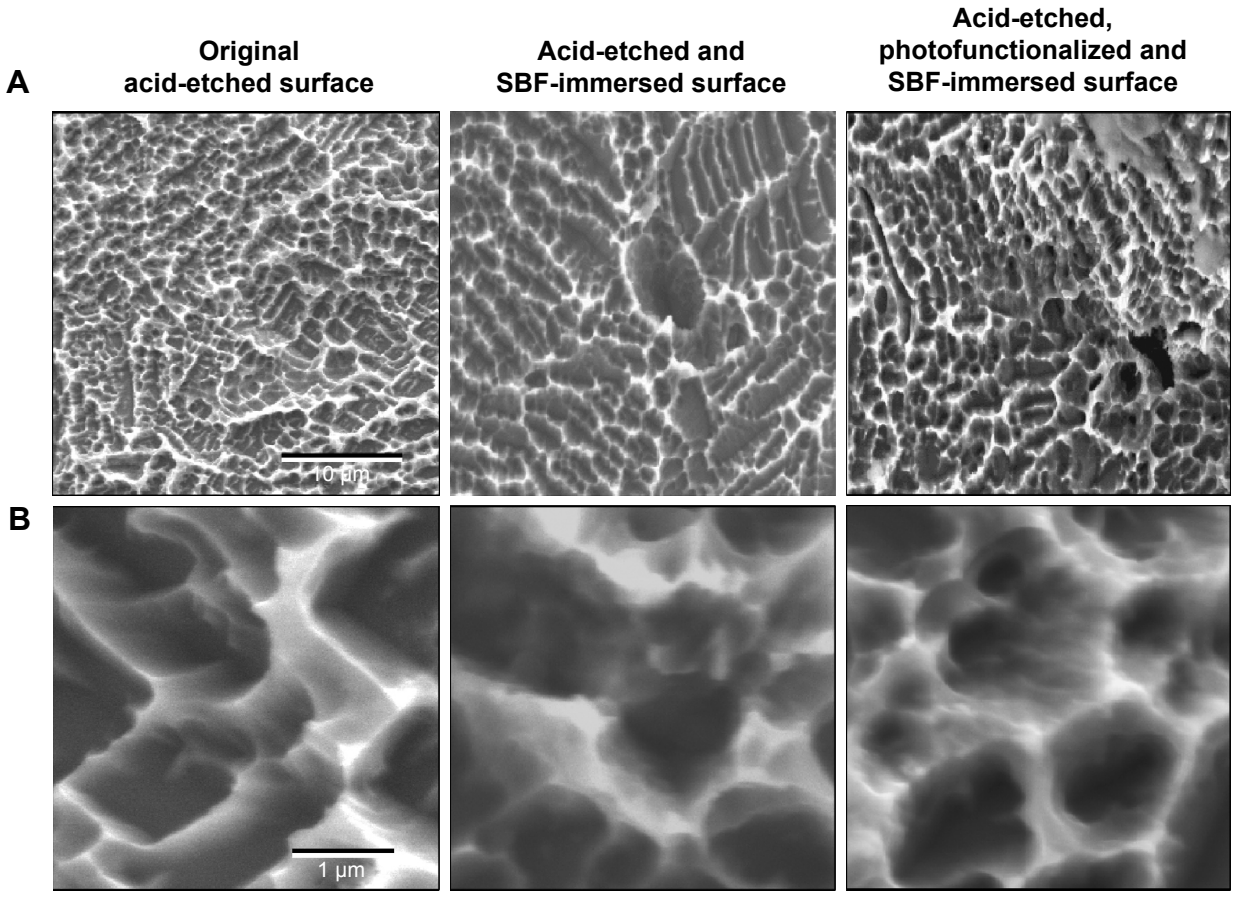

Figure 2 Surface morphology of titanium before and after immersion in SBF.
Notes: Low- (**A**) and high- (**B**) magnification SEM images of titanium disks after 1-day or 5-day immersion in SBF with or without pre-photofunctionalization. The titanium surface without SBF immersion is also presented for comparison.
Abbreviations: SEM, scanning electron microscopy; SBF, simulated body fluid.

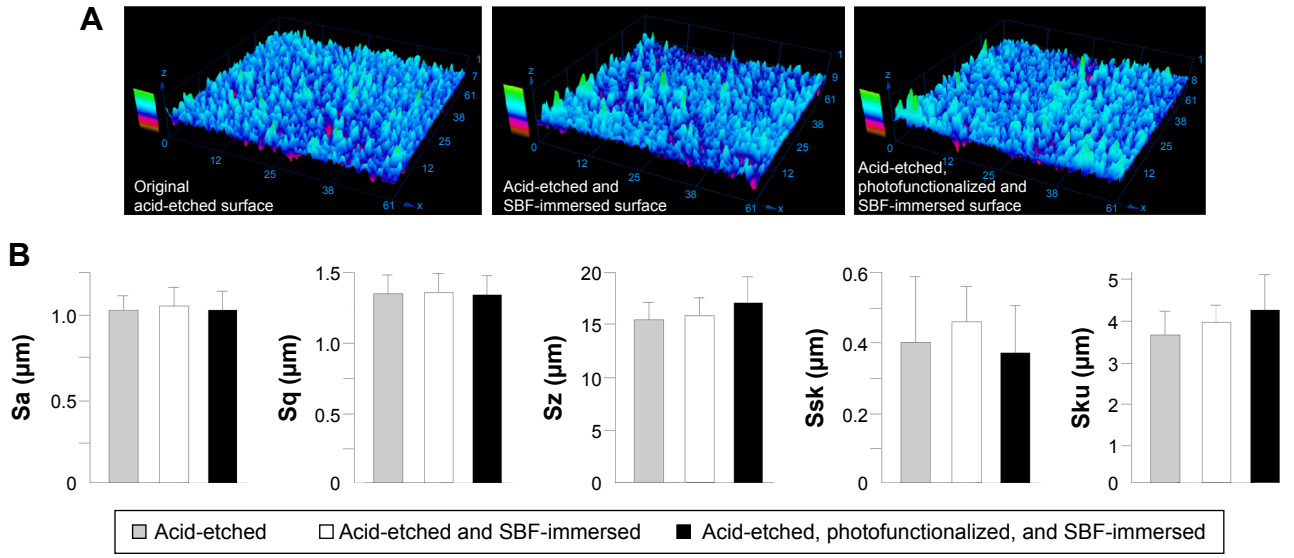

Figure 3 Surface morphological analysis of titanium disks after 1-day or 5-day immersion in SBF with or without pre-photofunctionalization.
Notes: The titanium surface without SBF immersion is also presented for comparison. (**A**) three-dimensional images obtained by laser profiling microscopy. (**B**) Calculated roughness parameters based on the images.
Abbreviations: SBF, simulated body fluid; Sa, average roughness; Sq, root-mean-square roughness; Sz, peak-to-valley roughness; Ssk, skewness roughness; Sku, kurtosis roughness.

that all roughness parameters were not significantly different among the three surfaces (Figure 3B).

XRD revealed an apatite-specific peak on photofunctionalized titanium after 1 day of SBF immersion (Figure 4A). An apatite-specific peak was present on as-made titanium after 5 days of SBF immersion, with photofunctionalized titanium showing an even higher peak. The peak intensity was approximately seven times greater and 2.5 times greater for photofunctionalized titanium than as-made titanium after 1 and 5 days of immersion, respectively (Figure 4A). After 1 day of immersion, the apatite intensity of photofunctionalized titanium was equivalent to that obtained for as-made titanium after 5 days of immersion. The amount of calcium deposition on titanium was significantly greater on photofunctionalized surfaces than as-made surfaces (Figure 4B). Thus, biomimetic apatite was successfully deposited at the nanoscale on micro-featured titanium surfaces.

Osteoblastic attachment and spreading behavior on nano-biomimetic apatite-coated titanium

Osteoblasts were cultured on biomimetic apatite-deposited titanium surfaces created by immersing as-made or photofunctionalized titanium disks for 1 day (Figure 5A). The number of osteoblasts attached during a 24-hour incubation was 30% greater for pre-photofunctionalized surfaces than as-made surface, which was confirmed by the confocal microscopic images depicting a higher number of cells on photofunctionalized surface (Figure 5B). Confocal microscopic images at day 1 of culture showed that cells were larger on pre-photofunctionalized surfaces than on as-made surfaces with more intense expression of vinculin (Figure 6A). The cytoskeletal development and the degree of stretching cell processes appeared advanced in cells on pre-photofunctionalized surfaces (Figure 6A).

Densitometric analysis of the confocal microscopic images confirmed that the cells spread larger on pre-photofunctionalized surface with upregulated expression of cytoskeletal actin and vinculin (Figure 6B).

Osteoblastic proliferation and phenotype on nano-biomimetic apatite-coated titanium

The number of cells propagated during culture was evaluated by measuring cell density at day 3. Cell density was significantly greater on photofunctionalized surfaces than on as-made surfaces (Figure 7A). Consistent with this, osteoblasts on photofunctionalized surfaces were more proliferative (Figure 7B). Osteoblastic ALP activity at day 10 was significantly greater on photofunctionalized than as-made surfaces (Figures 8A and B).

Discussion

Here we show that biomimetic apatite can be effectively and efficiently deposited on UV photofunctionalized titanium

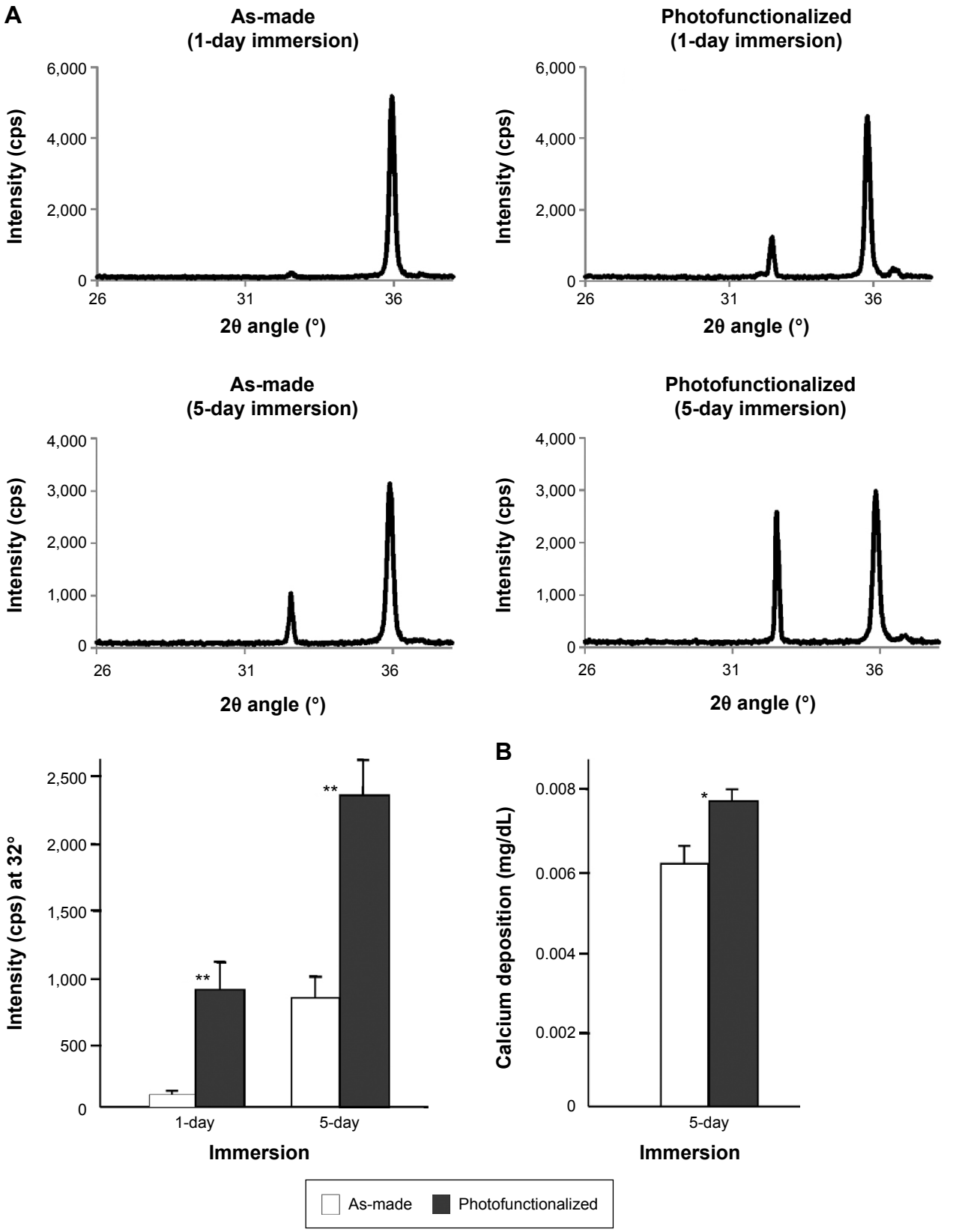

Figure 4 Calcium phosphate quantification on titanium disks after 1-day or 5-day immersion in SBF.

Notes: As-made and photofunctionalized titanium disks were compared. (**A**) XRD spectra and a histogram quantifying the intensity of apatite-specific signal at 32° (2θ angle). The XRD analysis as performed on three independent titanium samples for each group (n=3). (**B**) The amount of calcium phosphate measured by chemical detection. *$P<0.05$, **$P<0.001$, significant difference between as-made and photofunctionalized titanium.

Abbreviations: SBF, simulated body fluid; XRD, X-ray diffraction.

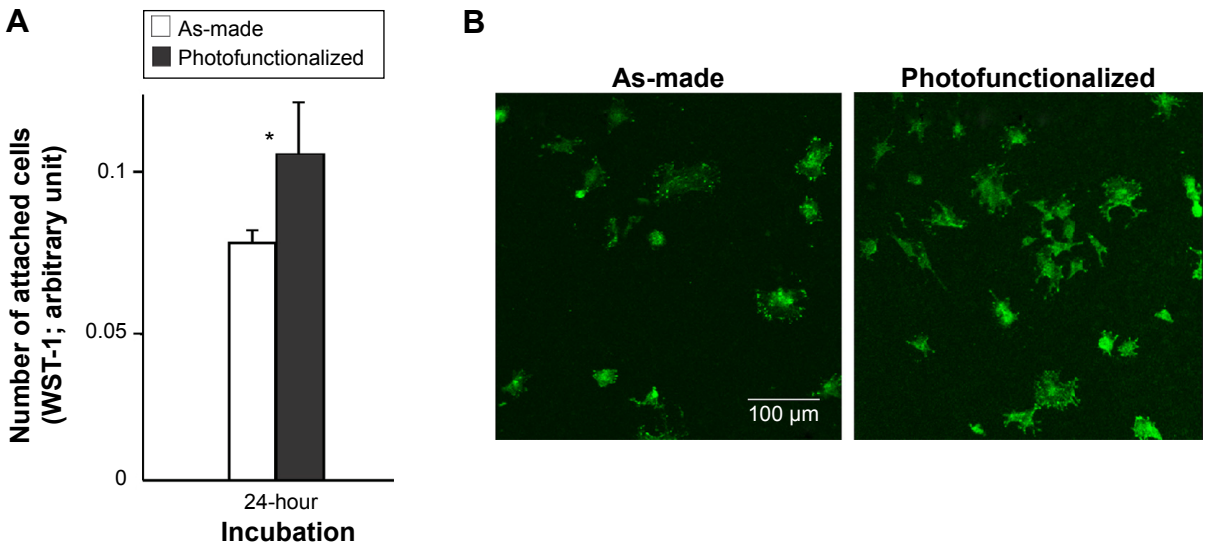

Figure 5 Osteoblast attachment to biomimetic apatite-deposited titanium disks.
Notes: (**A**) The number of attached cells during 24-hour incubation evaluated by WST-1 assay. *$P<0.05$, significant difference between as-made and photofunctionalized titanium. (**B**) Confocal microscopic images of osteoblasts.

surfaces. The quantity of apatite deposited on photofunctionalized titanium after 1 day of immersion in SBF was equivalent to that on as-made titanium after 5 days of immersion, indicating that the speed of the deposition was five times greater on photofunctionalized titanium. Apatite deposition with similar SBF has been reported to take 7 days,[11] while here it took only 1 day for an apatite peak to appear in XRD spectra of photofunctionalized titanium surfaces. Apatite deposition remained 2.5 times greater on photofunctionalized titanium than as-made titanium even after 5 days of immersion, indicating that photofunctionalization enabled a larger area of deposition as well as accelerating the process. Despite the large difference in apatite deposition caused by photofunctionalization, there was only a 20% difference in the amount of calcium deposition between the two surfaces, implying that photofunctionalization may have particularly accelerated the nucleation and crystallization of apatite.

Although the exact mechanism underlying enhanced apatite deposition is unclear, we propose the following model (Figure 9). First, we confirmed that photofunctionalized titanium surfaces are superhydrophilic and chemically clean. Superhydrophilicity resulted in inhibition of air bubble formation on photofunctionalized surfaces during SBF immersion. It was reasonable that the superhydrophilicity may have allowed a greater area of SBF contact with the titanium surface, leading to more apatite deposition. Second, the surface electrostatic status may have played a role in apatite deposition: hydrocarbon-free titanium surfaces are known to be electropositive, whereas as-made titanium surfaces bearing hydrocarbons are electro-neutral.[35,38] Electropositive photofunctionalized surfaces may attract more PO_4^{3-}, in turn facilitating Ca^{2+} recruitment. In contrast, as-made titanium surfaces have no active Ca^{2+} and PO_4^{3-} recruitment mechanism, and therefore these ions bond in solution rather than at the titanium interface. Consequently, the probability of apatite deposition at the titanium interface may have been higher on photofunctionalized surfaces. The distinct mechanism may also have resulted in the different rate of apatite crystallization. Another question is whether there was a difference in apatite bonding strength between as-made and photofunctionalized titanium. The apatite was intervened by hydrocarbon on as-made titanium surfaces, while it was directly deposited on photofunctionalized titanium surfaces (Figure 9). The potential delamination and dissolution of apatite coated on titanium have been ongoing issues. The interfacial strength of deposited apatite on photofunctionalized titanium as well as its crystallization mechanism would be of great interest in future studies.

The biological advantage of biomimetic apatite deposition on photofunctionalized titanium was confirmed in vitro. The cell attachment and initial cell behavior, including spreading and settling, were enhanced by photofunctionalization. This resulted in an enhanced functional phenotype of ALP activity. We also aimed to add nanoscale structure to titanium without altering the existing microscale morphology. Accordingly, the compartmental peak and trough configuration architecture of acid-etched titanium surface was maintained after apatite

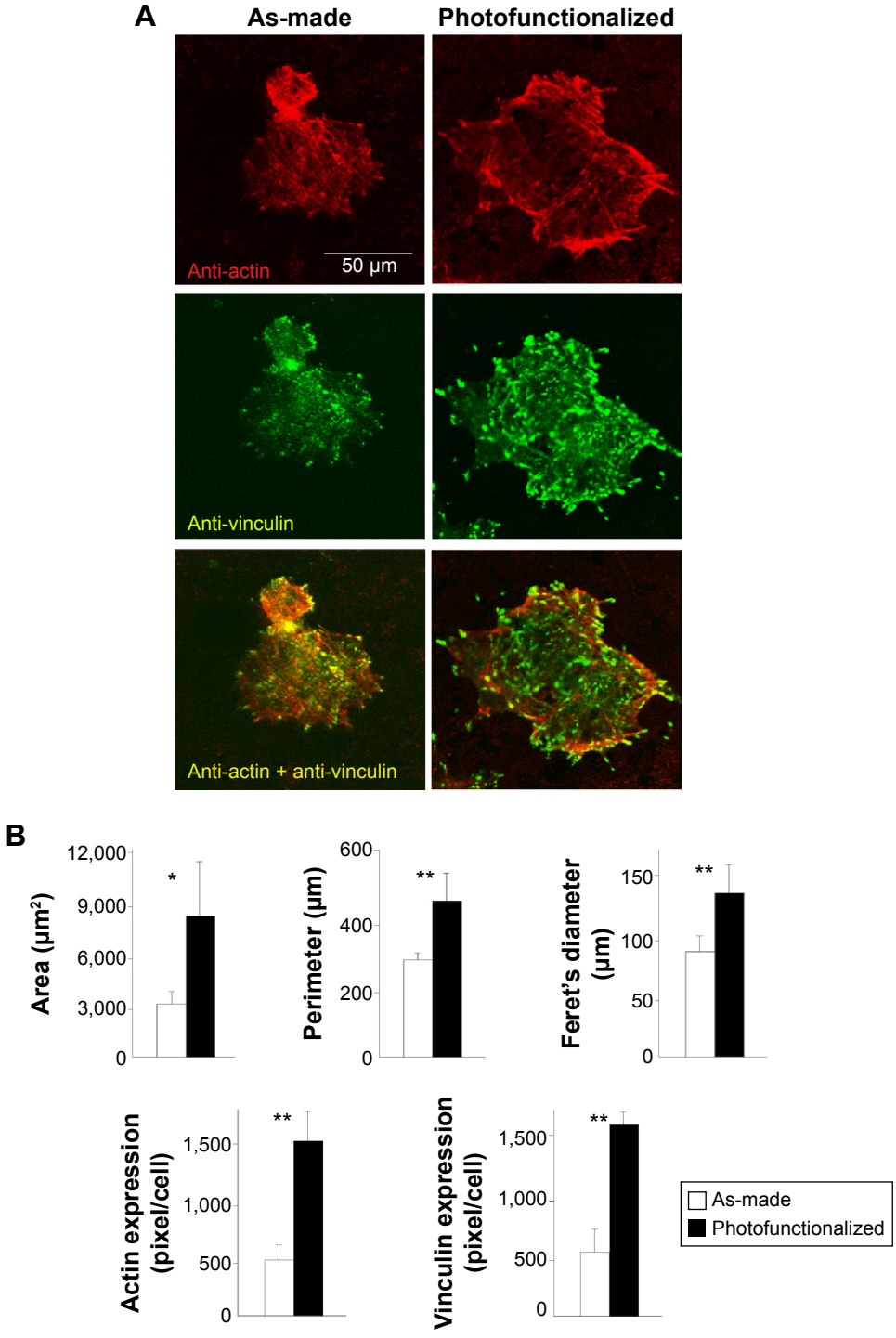

Figure 6 Osteoblast spreading and adhesion behavior on biomimetic apatite-deposited titanium disks.
Notes: (**A**) Confocal microscopic images of osteoblasts 24 hours after seeding, with immunochemical stain for cytoskeletal actin and adhesion protein, vinculin. (**B**) Quantified cytomorphometric parameters and expression levels of actin and vinculin. *$P<0.05$, **$P<0.001$, significant difference between as-made and photofunctionalized titanium.

deposition, which was corroborated by unchanged surface roughness parameters. Thus, photofunctionalization-assisted biomimetic apatite coating produced a unique morphology representing the coexistence of micro- and nanoscale structures.

In addition to improving the efficiency of biomimetic apatite deposition on titanium, we also uncovered a new mechanism underpinning the enhanced biological capability and osteoconductivity of photofunctionalized titanium. Increased recruitment, attachment, retention, spread, and

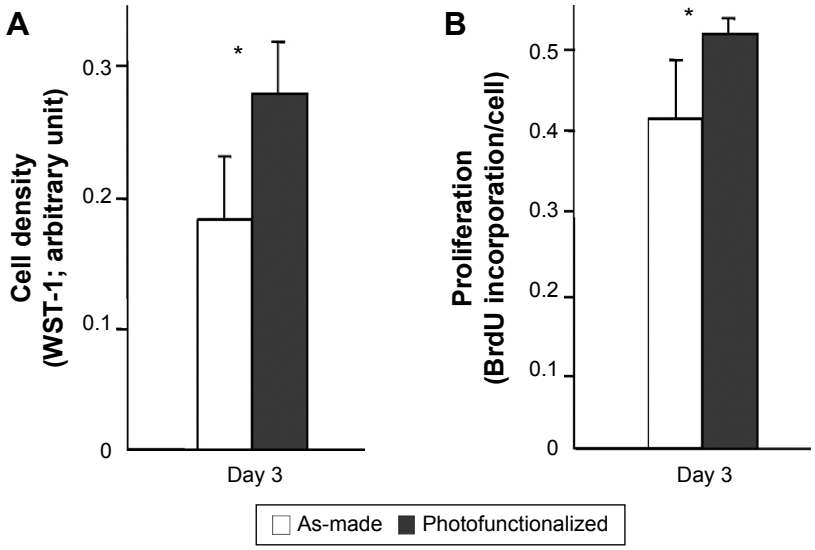

Figure 7 Osteoblast proliferative activity on biomimetic apatite-deposited titanium.
Notes: (**A**) Cell density evaluated at day 3 by WST-1 assay. (**B**) Cell proliferation evaluated by BrdU incorporation into DNA at day 3. *$P<0.05$, significant difference between as-made and photofunctionalized titanium.

functional phenotype of osteoblasts are known to contribute to increased bone-implant contact around photofunctionalized titanium. This study unveiled that photofunctionalization promotes apatite deposition on titanium even without osteoblasts. Biomineralization is essential for bone generation and regeneration and, therefore, bone-implant integration. The present results provide novel biochemical evidence of the increased bioactivity of photofunctionalized titanium. In fact, a recent study demonstrated the remarkable bone generation around photofunctionalized titanium, as represented by the far-reaching, extensive, and faster bone formation, and proposed to define its active osteoconduction capability as opposed to passive or inert osteoconductivity of ordinary titanium.[43] This proposal has been supported by the disparate perspective of active biomineralization.

Conclusion

Here we examined the effect of photofunctionalization on the efficiency of biomimetic apatite deposition on micro-roughened titanium and its effect on biological capability. Photofunctionalization accelerated the apatite deposition on titanium. Apatite was deposited in nodular form on existing micro-roughened structures without affecting the innate micro-configuration. The attachment, spreading, settling, and

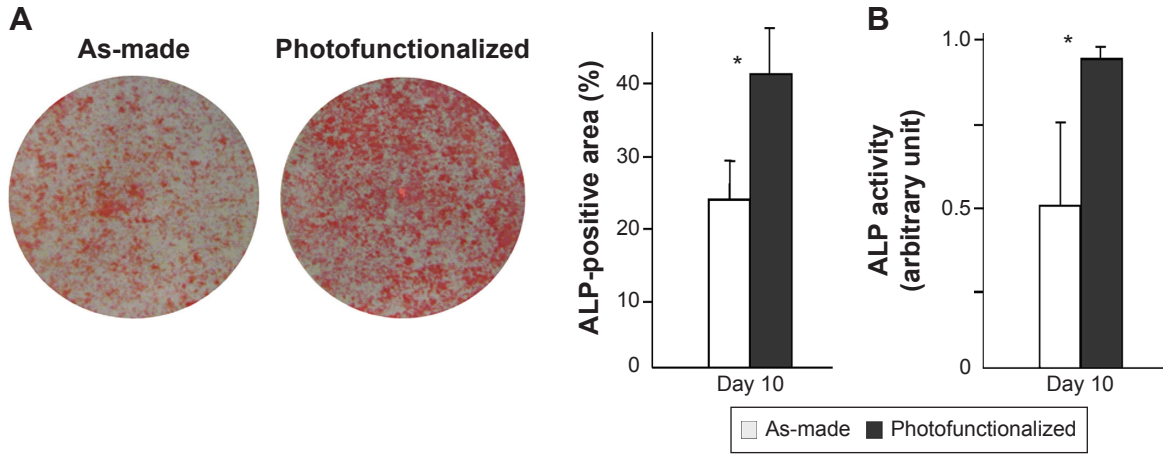

Figure 8 ALP activity of osteoblasts at day 10 on biomimetic apatite-deposited titanium disks.
Notes: (**A**) Images after ALP staining and densitometrically quantified ALP using the images. (**B**) ALP activity colorimetrically evaluated. *$P<0.05$, significant difference between as-made and photofunctionalized titanium.
Abbreviation: ALP, alkaline phosphatase.

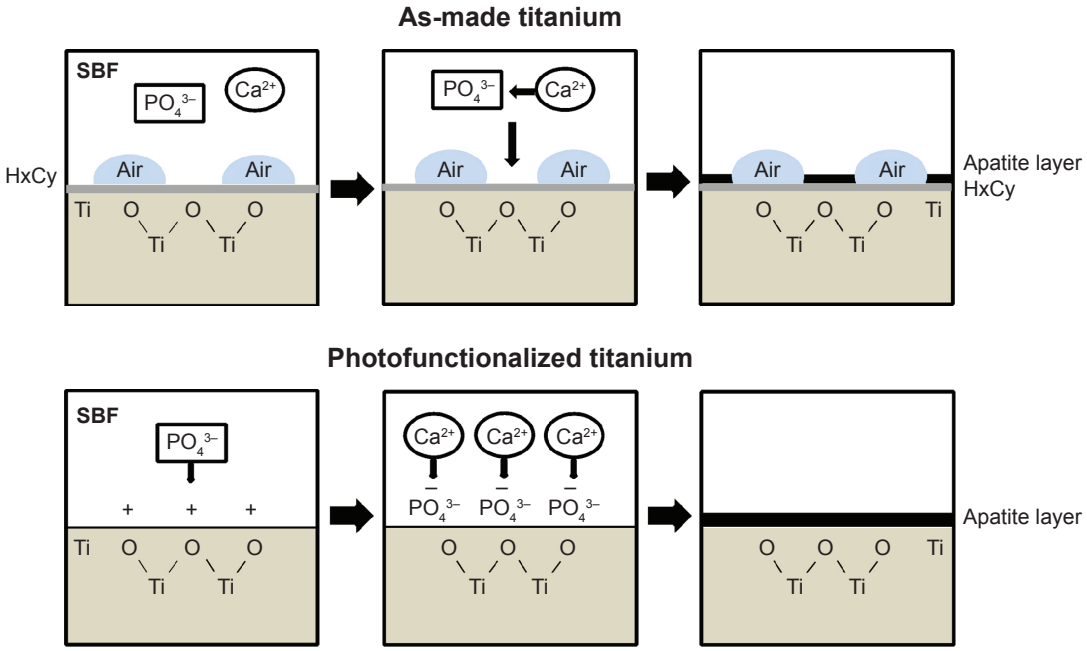

Figure 9 Proposed mechanism of nano-biomimetic apatite deposition on as-made and photofunctionalized titanium surfaces.
Notes: Direct deposition of apatite takes place on photofunctionalized titanium surfaces, whereas the hydrocarbon layer is intervened between apatite and titanium on as-made titanium surfaces. The area of apatite deposition is also increased on photofunctionalized titanium because of the elimination of surface air bubbles.
Abbreviation: SBF, simulated body fluid.

subsequent proliferation and function of osteoblasts were promoted on apatite-coated titanium with photofunctionalization. Thus, photofunctionalization enhanced the deposition of nanoscale apatite on titanium, establishing a novel photofunctionalization-assisted biomimetic apatite deposition to produce better titanium surfaces.

Acknowledgment

This work was partially supported by a research gift from USHIO INC.

Disclosure

The authors report no conflicts of interest in this work.

References

1. Sandrini E, Giordano C, Busini V, Signorelli E, Cigada A. Apatite formation and cellular response of a novel bioactive titanium. *J Mater Sci Mater Med*. 2007;18(6):1225–1237.
2. Kokubo T, Kim HM, Kawashita M, Nakamura T. Bioactive metals: preparation and properties. *J Mater Sci Mater Med*. 2004;15(2):99–107.
3. Miyaza T, Kim HM, Kokubo T, Ohtsuki C, Kato H, Nakamura T. Mechanism of bonelike apatite formation on bioactive tantalum metal in a simulated body fluid. *Biomaterials*. 2002;23(3):827–832.
4. Wang XX, Hayakawa S, Tsuru K, Osaka A. A comparative study of in vitro apatite deposition on heat-, H(2)O(2)-, and NaOH-treated titanium surfaces. *J Biomed Mater Res*. 2001;54(2):172–178.
5. Kim HM, Miyaji F, Kokubo T, Nakamura T. Bonding strength of bonelike apatite layer to Ti metal substrate. *J Biomed Mater Res*. 1997;38(2):121–127.
6. Ajami E, Aguey-Zinsou KF. Calcium phosphate growth at electropolished titanium surfaces. *J Funct Biomater*. 2012;3(2):327–348.
7. Havitcioglu H, Cecen B, Pasinli A, Yuksel M, Aydin I, Yildiz H. In vivo investigation of calcium phosphate coatings on Ti6-Al-4V alloy substrates using lactic acid – sodium lactate buffered synthetic body fluid. *Acta Orthop Traumatol Turc*. 2013;47(6):417–22.
8. Uchida M, Kim HM, Kokubo T, Fujibayashi S, Nakamura T. Effect of water treatment on the apatite-forming ability of NaOH-treated titanium metal. *J Biomed Mater Res*. 2002;63(5):522–530.
9. Pattanayak DK, Kawai T, Matsushita T, Takadama H, Nakamura T, Kokubo T. Effect of HCl concentrations on apatite-forming ability of NaOH-HCl- and heat-treated titanium metal. *J Mater Sci Mater Med*. 2009;20(12):2401–2411.
10. Cui X, Kim HM, Kawashita M, et al. Effect of hot water and heat treatment on the apatite-forming ability of titania films formed on titanium metal via anodic oxidation in acetic acid solutions. *J Mater Sci Mater Med*. 2008;19(4):1767–1773.
11. Wang XX, Yan W, Hayakawa S, Tsuru K, Osaka A. Apatite deposition on thermally and anodically oxidized titanium surfaces in a simulated body fluid. *Biomaterials*. 2003;24(25):4631–1437.
12. Gross KA, Young CJ, Beck MA, et al. Characterization and dissolution of functionalized amorphous calcium phosphate biolayers using single-splat technology. *Acta Biomater*. 2011;7(5):2270–2275.
13. Saber-Samandari S, Gross KA. The use of thermal printing to control the properties of calcium phosphate deposits. *Biomaterials*. 2010;31(25):6386–6393.
14. Saber-Samandari S, Alamara K, Saber-Samandari S. Calcium phosphate coatings: Morphology, micro-structure and mechanical properties. *Ceramics International*. 2014;40(1):563–572.
15. Aita H, Ogawa T. Nanotechnology for Implant Dentistry. *Journal of Japanese Society for Biomaterials*. 2008;26:234–246.
16. Dalby MJ, Gadegaard N, Tare R, et al. The control of human mesenchymal cell differentiation using nanoscale symmetry and disorder. *Nat Mater*. 2007;6(12):997–1003.
17. Balasundaram G, Webster TJ. Nanotechnology and biomaterials for orthopedic medical applications. *Nanomedicine (Lond)*. 2006;1(2):169–176.

18. Barrere F, Snel MM, van Blitterswijk CA, de Groot K, Layrolle P. Nano-scale study of the nucleation and growth of calcium phosphate coating on titanium implants. *Biomaterials*. 2004;25(14):2901–2910.
19. Christenson EM, Anseth KS, van den Beucken JJ, et al. Nanobiomaterial applications in orthopedics. *J Orthop Res*. 2007;25(1):11–22.
20. Cooper LF, Zhou Y, Takebe J, et al. Fluoride modification effects on osteoblast behavior and bone formation at TiO2 grit-blasted c.p. titanium endosseous implants. *Biomaterials*. 2006;27(6):926–936.
21. Cooper LF. A role for surface topography in creating and maintaining bone at titanium endosseous implants. *J Prosthet Dent*. 2000;84(5): 522–534.
22. Mendonca G, Mendonca DB, Aragao FJ, Cooper LF. Advancing dental implant surface technology – from micron- to nanotopography. *Biomaterials*. 2008;29(28):3822–3835.
23. Nishimura I, Huang Y, Butz F, Ogawa T, Lin A, Wang CJ. Discrete deposition of hydroxyapatite nanoparticles on a titanium implant with predisposing substrate microtopography accelerated osseointegration. *Nanotechnology*. 2007;18:245101.
24. Yamada M, Ueno T, Tsukimura N, et al. Bone integration capability of nanopolymorphic crystalline hydroxyapatite coated on titanium implants. *Int J Nanomedicine*. 2012;7:859–873.
25. Cooper LF. Biologic determinants of bone formation for osseointegration: clues for future clinical improvements. *J Prosthet Dent*. 1998;80(4): 439–449.
26. Stanford CM. Biomechanical and functional behavior of implants. *Adv Dent Res*. 1999;13:88–92.
27. Wennerberg A, Albrektsson T. Suggested guidelines for the topographic evaluation of implant surfaces. *Int J Oral Maxillofac Implants*. 2000;15(3):331–344.
28. Wennerberg A, Albrektsson T. On implant surfaces: a review of current knowledge and opinions. *Int J Oral Maxillofac Implants*. 2010; 25(1):63–74.
29. Dalby MJ, McCloy D, Robertson M, Wilkinson CD, Oreffo RO. Osteoprogenitor response to defined topographies with nanoscale depths. *Biomaterials*. 2006;27(8):1306–1315.
30. Ogawa T. UV-photofunctionalization of titanium implants. *Oral and Craniofacial Tissue Engineering*. 2012;2:151–158.
31. Att W, Ogawa T. Biological aging of implant surfaces and their restoration with ultraviolet light treatment: a novel understanding of osseointegration. *Int J Oral Maxillofac Implants*. 2012;27(4):753–761.
32. Att W, Hori N, Iwasa F, Yamada M, Ueno T, Ogawa T. The effect of UV-photofunctionalization on the time-related bioactivity of titanium and chromium-cobalt alloys. *Biomaterials*. 2009;30(26):4268–4276.
33. Aita H, Hori N, Takeuchi M, et al. The effect of ultraviolet functionalization of titanium on integration with bone. *Biomaterials*. 2009; 30(6):1015–1025.
34. Hori N, Iwasa F, Tsukimura N, et al. Effects of UV photofunctionalization on the nanotopography enhanced initial bioactivity of titanium. *Acta Biomater*. 2011;7(10):3679–3691.
35. Iwasa F, Hori N, Ueno T, Minamikawa H, Yamada M, Ogawa T. Enhancement of osteoblast adhesion to UV-photofunctionalized titanium via an electrostatic mechanism. *Biomaterials*. 2010;31(10):2717–2727.
36. Iwasa F, Tsukimura N, Sugita Y, et al. TiO2 micro-nano-hybrid surface to alleviate biological aging of UV-photofunctionalized titanium. *Int J Nanomedicine*. 2011;6:1327–1341.
37. Att W, Hori N, Takeuchi M, et al. Time-dependent degradation of titanium osteoconductivity: an implication of biological aging of implant materials. *Biomaterials*. 2009;30(29):5352–5363.
38. Hori N, Ueno T, Minamikawa H, et al. Electrostatic control of protein adsorption on UV-photofunctionalized titanium. *Acta Biomater*. 2010; 6(100):4175–4180.
39. Hori N, Ueno T, Suzuki T, et al. Ultraviolet light treatment for the restoration of age-related degradation of titanium bioactivity. *Int J Oral Maxillofac Implants*. 2010;25(1):49–62.
40. Yamada M, Miyauchi T, Yamamoto A, et al. Enhancement of adhesion strength and cellular stiffness of osteoblasts on mirror-polished titanium surface by UV-photofunctionalization. *Acta Biomater*. 2010;6(12): 4578–4588.
41. Lee JH, Ogawa T. The biological aging of titanium implants. *Implant Dent*. 2012;21(5):415–421.
42. Saruwatari L, Aita H, Butz F, et al. Osteoblasts generate harder, stiffer, and more delamination-resistant mineralized tissue on titanium than on polystyrene, associated with distinct tissue micro- and ultrastructure. *J Bone Miner Res*. 2005;20(11):2002–2016.
43. Hirota M, Ikeda T, Tabuchi M, Nakagawa K, Park W, Ishijima M, et al. Bone generation profiling around photofunctionalized titanium mesh. *Int J Oral Maxillofac Implants*. Epub.